Expanding Orbitrap collision cross section measurements to native protein applications through kinetic energy and signal decay analysis

Virginia K. James,[1] James D. Sanders,[1] Konstantin Aizikov,[2] Kyle L. Fort,[2] Dmitry Grinfeld ,[2] Alexander Makarov,[2,3] Jennifer S. Brodbelt [1]*

1. Department of Chemistry, The University of Texas at Austin, Austin, TX 78712
2. Thermo Fisher Scientific, Bremen, Germany 28199
3. Biomolecular Mass Spectrometry and Proteomics, Bijvoet Center for Biomolecular Research and Utrecht Institute for Pharmaceutical Sciences, University of Utrecht, Utrecht 3584, The Netherlands

*Correspondence to: jbrodbelt@cm.utexas.edu

Abstract

The measurement of collision cross sections (CCS, σ) offers supplemental information about sizes and conformations of ions beyond mass analysis alone. We have previously shown that CCSs can be determined directly from the time-domain transient decay of ions in an Orbitrap mass analyzer as ions oscillate around the central electrode and collide with neutral gas, thus removing them from the ion packet. Herein, we develop the modified hard collision model, thus deviating from prior FT-MS hard sphere model, to determine CCSs as a function of center-of-mass collision energy in the Orbitrap analyzer. With this model, we aim to increase the upper mass limit of CCS measurement for native-like proteins, characterized by low charge states and presumed to be in more compact conformations. We also combine CCS measurements with collision induced unfolding and MS/MS experiments to monitor protein unfolding and disassembly of protein complexes and measure CCSs of ejected monomers from protein complexes.

Introduction

Protein function is directly modulated by its structure, as defined by an array of secondary structural motifs, such as alpha helices and beta sheets, that organize into dynamic three-dimensional structures mediated by networks of intramolecular interactions. As such, understanding how variations in the conformations of proteins influence their functions depends critically on the ability to determine their shapes and sizes. Auxiliary to the important correlation between structure and function is the interesting dichotomy between the tertiary structures of proteins in solution versus the gas phase. In the gas phase, sizes of proteins are inferred by their collision cross sections (CCS). Measurement of CCSs of gas-phase protein ions has become a valuable and increasingly routine aspect of a wide variety of bioanalytical workflows.[1–5] Traditionally these measurements may be directly made using drift tube ion mobility (IM)[6] analyzers, typically coupled to a mass spectrometer.[7,8] More recently, protocols have been developed to perform CCS measurements using traveling wave[9–11] and trapped ion mobility[12–15] instruments through calibration with ions of known CCS. On commercial platforms, these IM set-ups are typically paired with time-of-flight (TOF) mass spectrometers, but the need for higher mass resolving power and access to advanced tandem mass spectrometry (MS/MS) methods has led to the development of gating and multiplexing techniques that enable fast IM separations to be compatible with the scan times of slower mass analyzers such as ion trap and Fourier transform (FT)-based mass analyzers.[2,16–19] These techniques have expanded the capabilities of IM-MS for the analysis of larger and more complex biomolecules.[2] While some commercial IM systems, such as trapped ion mobility spectrometry, have CCS limits of approximately 4,000 Å^2,[20] corresponding to protein mass of around 25-60 kDa depending on the charge state and whether the protein is native-like or denatured, many other home-built and commercial systems, such as drift tube and traveling wave ion mobility spectrometers, have approached the upper mass limit of the ionization sources used and the mass spectrometer itself.[21] For example, protein complexes up to 4 MDa and 800 kDa have been analyzed on drift tube[22] and traveling wave IM instruments,[23] respectively. More recently a home-built trapped ion mobility spectrometer has also approached an 800 kDa mass limit.[24] The CCSs determined for these MDa complexes have ranged up to 914,000 Å^2 on drift tube systems.[21]

Using a distinctly different approach, CCS measurements have also been realized through analysis of the decay rate of the time domain signal from FT mass analyzers.[25,26] Using either the width of frequency domain peaks[27–31] or direct analysis of the time domain transient signal,[32] the CCS of small molecules,[27,33,34] peptides,[29,31] and intact proteins[31,32] have been measured on Fourier transform ion cyclotron resonance (FT-ICR) mass spectrometers. CCS measurements of small molecules and peptides have also been

performed in charge detection mass spectrometers[35] and electrostatic linear ion traps.[36] Moreover, building on previous work,[37] our group demonstrated that direct measurement of the time domain signal produced by an Orbitrap™ mass analyzer could be used to estimate CCSs of intact proteins up to the mass of holo myoglobin (17.5 kDa).[38] While these methods do not provide physical separation of isobaric or isomeric species, they offer compelling alternative routes for determining sizes of increasingly large proteins with little or no instrument modifications, expanding the accessibility and workflows of CCS determinations. It should also be noted that for the methods used to estimate CCS on FT-MS platforms (inclusive of both FT-ICR and Orbitrap analyzers), the ion kinetic energies are much higher (> 1 keV per charge) compared to the collisions in conventional IM methods (typically less than 1 eV[39,40]). Owing to these high kinetic energies, the long range interactions characteristic of the Langevin model, a model relevant for many ion mobility methods in which ions experience multiple collisions and polarizability of the gas may cause structural changes that influence CCS, are insignificant.[41–43] Instead, the hard sphere collision cross-section model is more appropriate for Orbitrap CCS experiments. In the hard sphere collision model, the cross-section is described by the effective radius of an ion and which may be averaged over all possible orientations. Thus, CCS values measured in the keV range are not expected to duplicate those in the eV range. While the hard sphere collision model in theory should yield lower CCS values than the Langevin model,[25] in practice we have found that Orbitrap CCSs are generally within 10% of ion mobility CCSs, likely owing to the need to calibrate the pressure of the Orbitrap chamber with a protein ion of a single known conformer by ion mobility in order to obtain CCS.[38,44]

Regardless of whether the ion signal decay rate is measured in the frequency or time domain, the theory underlying CCS measurements in FT mass analyzers is predicated on the assumption that a single ion-neutral gas collision occurring inside the analyzer will always remove the ion from the orbiting ion packet (either *via* ion fragmentation or scattering).[25,37] As each ion is no longer detected after such a collision, secondary and tertiary structural changes caused by the collision will not be reflected in the CCS measurement. This method contrasts with conventional ion mobility experiments in which ions are detected after multiple collisions and therefore the resulting CCSs may reflect multiple structural changes. As smaller sized protein ions are unable to survive collisions at such energies, the rate of collisions is reflected adequately in the decay rate of the induced current signal. The number of survived ions of a particular sort drops exponentially with time as

$$N(t) = N_0 e^{-ct} \quad (1)$$

where N_0 is the number of injected ions, and *t* is the time in seconds. The coefficient c may be determined from the experimental data by fitting an exponential function to the transients. On the other hand, this coefficient represents the reciprocal mean lifetime of an ion, and the CCS may be calculated as [37,38]

$$CCS = \frac{c}{f_z L\, n_g} \tag{2}$$

Here, f_z is the oscillation frequency of an ion in the *Z* (axial) dimension, *L* is the path length of a single oscillation, and n_g is the number density of the neutral gas related to the pressure (*p*) and temperature (*T*) along with the Boltzman constant (k_b) as $n_g = p/k_b T$. As previously discussed, the neutral gas density must be calculated using the decay rate and ion mobility CCS of an ion with a single known conformer by ion mobility. Since the pathlength of an ion is dependent only on the instrument, the calibrated collision cross section can be calculated using equation 3 below.

$$CCS^{unknown} = \frac{c^{unknown} f_z^{calibrant}}{c^{calibrant} f_z^{unknown}} * CCS^{calibrant} \tag{3}$$

While this method afforded CCS values that agreed within 7% of CCS values from IM measurements for proteins of small (8.5 kDa) to moderate (17.5 kDa) size in our previous study,[38] there are several factors that shed doubt on the feasibility of the method and its underlying assumptions for even larger proteins, particularly ones in low charge states with higher *m/z*. First, proteins containing a larger number of residues have more degrees of freedom over which the internal energy transferred during a collision can be distributed. If this energy is effectively distributed across many vibrational modes, there may be insufficient energy to cause dissociation and the ion will survive the collision. Second, an ion's kinetic energy has been shown to affect CCS measurements in FT-ICR instruments,[45] an outcome reflecting that an ion has a greater chance of surviving a collision (*i.e.*, not dissociating) when the ion has lower kinetic energy. In Orbitraps, single ion studies have shown that large complexes with molecular masses of hundreds of kDa or even MDa can continue to be detected even after a large number of collisions in the Orbitrap analyzer.[46] In light of these factors, the effect of ion kinetic energy should also be considered in Orbitrap CCS measurements. In an Orbitrap analyzer, the kinetic energy that is imparted to an ion during injection from the C-trap to the Orbitrap analyzer is equal to the acceleration voltage times the charge state. Proteins in low charge states, such as ones sprayed from solutions of high ionic strength to retain native-like conformations, may have a substantially smaller numbers of charges (*e.g.*, less than half) and therefore smaller kinetic energies compared to denatured proteins in high charge states. If one or both factors (degrees of freedom and kinetic energy) cause a significant number of ions to survive collisions in the trap, the model of the hard sphere cross-section will no longer apply as not every collision within the geometrical size of an ion results in the ion's removal from the bunch. Therefore, the decay rate of the

time domain signal will not accurately reflect the collision rate and therefore cannot be used to measure ion CCS. Here, we developed an alternative model (termed the "modified hard sphere collision model") to describe these lower kinetic energy collisions through a systematic evaluation of ion dynamics related to mass and kinetic energy in an Orbitrap mass spectrometer with the goal of extending the application of CCS measurements to larger proteins and protein complexes.

Methods

Equine heart myoglobin, carbonic anhydrase (bovine), and β-lactoglobulin A (bovine) were purchased from Sigma-Aldrich (St. Louis, MO, USA). Streptavidin (*Streptomyces avidinii*) was purchased from ProteoChem (Hurricane, UT, USA), and superoxide dismutase (Bovine) was purchased from MP Biomedical (Irvine, CA, USA). Membrane scaffold proteins (ΔH5 and D1T0) were provided by the Marty lab[47], and LC-MS grade water and methanol was purchased from Merck Millipore (Billerica, MA, USA). For experiments involving native-like charge states, proteins were diluted in a 100 mM ammonium acetate buffer to a final concentration of 5 μM and desalted with Micro Bio-Spin™ P-6 Gel Columns (Bio-Rad Laboratories Inc., Hercules, CA). For experiments with denaturing conditions, proteins were diluted in a denaturing 1:1 water–methanol solution containing 0.1% formic acid to a final concentration of 5 μM without further purification. For experiments requiring supercharging or charge reducing to generate a broader range of charge states, 10-40 mM of *m*-nitrobenzyl alcohol or triethyl ammonium acetate, respectively, were used.

Instrumentation

All experiments were performed on a Thermo Scientific™ Q Exactive™ HF-X quadrupole-Orbitrap mass spectrometer (Bremen, Germany) with Biopharma option, which was modified to collect two-second-long transients, corresponding to a resolution of 960,000 at *m/z* 200. This mass spectrometer was also modified to perform ultraviolet photodissociation (UVPD) with a 500 Hz, 193 nm Coherent® ExciStar excimer laser (Santa Cruz, CA) in the HCD cell as previously described.[48–50] Ions were generated by nano electrospray ionization using Au/Pt-coated borosilicate emitters fabricated in-house and using a spray voltage of 0.8-1.2 kV. During collision induced unfolding (CIU) experiments, ions were subjected to increasing amounts of in-source dissociation. Multimeric proteins were subjected to HCD or UVPD in the HCD cell in order to generate monomers for some of the experiments, as described later. For most measurements of Orbitrap CCSs, selected charge states of each protein were isolated in the quadrupole with an isolation width of 3-5 *m/z*, including the CIU experiments in which the precursor was isolated after

activation. In some cases, monomers were not isolated after disassembly of multimer proteins by HCD or UVPD. For those experiments, a wide range selected ion monitoring (SIM) method was employed for measurement of Orbitrap CCS.[44] The wide-SIM method involves Orbitrap CCS measurements of 2-4 abundant charge states at the same time. This method allows simultaneous analysis of multiple different ions or charge states but may result in modest overestimation of CCS owing to space charge effects between charge states, as previously described.[44] Ion injection time was optimized for each charge state by varying the ion injection time and finding the ion injection time that gave the lowest decay rate. As previously described, having too few or too many ions injected at once may cause artificially inflated decay rates which yield over-estimated CCS values.[38,44] The C-trap gas pressure was set low (0.1 to 1.0 values, corresponding to 8E-11 to 1E-10 mBar measuring using the UHV gauge), which was optimized to provide measurable signal decay for each peak. Ion mobility CCSs were collected using a home-built atmospheric pressure drift tube as previously described.[49,51,52] This drift tube consists of a 10 cm drift region and 10 cm desolvation region, the latter of which causes lower charge states than those produced by direct electrospray ionization, thus requiring the need for supercharging (IM experiments) and charge reducing (Orbitrap CCS experiments) additives to obtain comparable charge states. Specific charge states were not isolated for the IM experiments.

Data Acquisition and Processing

A custom license provided by Thermo Fisher Scientific allowed the collection of transient data. Transient data was processed as previously described for Orbitrap CCS measurements using the direct decay profile fitting method.[38,44] Briefly, the time-domain transient was recorded, then Fourier transformed to generate a frequency spectrum. The complex frequency domain data corresponding to peaks of a single charge state in the resulting frequency spectrum were shifted to zero frequency, and subjected to inverse Fourier transform to yield a filtered time domain transient signal which was fit to an exponential decay function (**Figure S1**). All CCS data were calibrated to ubiquitin (9+ charge state) collected using denaturing solution conditions or myoglobin (8+ charge state) acquired using native-like solution conditions. All data were calibrated to data collected at the same pressure and on the same day, and the CCS values of the calibrant proteins are given in **Table S1**. Orbitrap CCSs for ions above *m/z* 2,200 were corrected using the correction factor described in the supporting information.

Drift tube ion mobility data was processed as previously reported.[49] Extracted ion chromatograms from the sweeps were produced for each charge state and imported in a custom Matlab script for Fourier transformation. The complex FT data was processed in magnitude mode to generate arrival time

distributions. From the arrival time, pressure, and temperature of the drift tube, the IM CCS was directly determined.[53]

Results and Discussion

Inherent mass and size limitations of Orbitrap CCS measurements

When examining the upper mass limit of ions for which CCS values can be determined in an Orbitrap analyzer, fundamental limitations in signal measurements must be considered. Even in low charge states, proteins in the mass range examined here have elaborate isotope profiles. As these isotopic ions are too close in *m/z* space to be isolated separately, the transient signal will have regions of constructive and destructive interference. The higher intensity, constructive interference regions are known as beats,[37] and it is the maxima of each beat that is measured for signal decay. The time between the subsequent beats (T_{beats}) is equal to the inverse frequency difference of two isotopic states:

$$T_{beats} = \left\{ f\left(\frac{m}{z}\right) - f\left(\frac{m+1}{z}\right) \right\}^{-1} \cong \left| \frac{\partial f}{\partial m} \right|^{-1} = \frac{2}{C} \frac{m^{3/2}}{z^{1/2}} \quad (4)$$

where $f\left(\frac{m}{z}\right) = \frac{C}{\sqrt{m/z}}$ is the oscillation frequency of an ion with a given *m/z* ratio and C is a constant defined by the electric field strength in the analyzer.[37] As signal decay is fit to an exponential function to determine the decay rate, the raw transient must have at least three full beats because the first beat of the transient is distorted at the very beginning of the acquisition by saturation of the preamplifier following the high-voltage pulse on the central electrode. Therefore, the acquisition time T must be longer than $2 \times T_{beats}$. Larger and less charged proteins require longer times of acquisition (**Scheme 1**). The maximum amount of time that transients can be acquired is limited by hardware and varies from one to four seconds on modified Orbitrap platforms.

Another consideration when acquiring transients of larger proteins is that their decay rates will be greater than decay rates of smaller ions at the same pressure due to the larger CCS when assuming that the hard sphere model is valid. If at least three beats are not observed in the transient (**Figure S2**), then a decay constant cannot be determined. Thus, the pressure must be modulated so that it is low enough to allow detection of at least three beats but sufficiently high so that decay in beat signal is confidently observed over the time of the transient. In essence, this means that the resolution must be at least twice better than the minimum required to resolve the isotopic structure, whether the resolution is limited by the acquisition time, ion mass, or the pressure (collisional decay). This relationship between pressure and ability to measure a decay constant is further complicated by differences in beat period, *i.e.*,

an ion with a short beat period and large CCS may be measurable while an ion with a long beat period and the same CCS is not measurable.

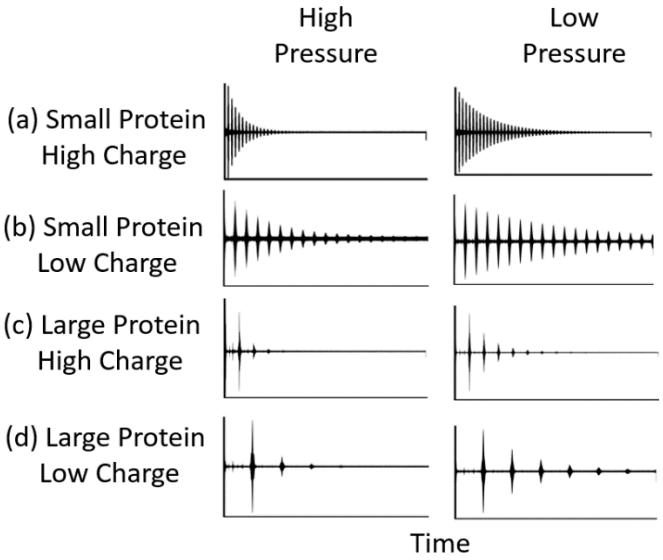

Scheme 1. Impact of pressure in an Orbitrap analyzer on transient decay and beat pattern as a function of protein mass and charge. (a, b) Small proteins have a high number of closely spaced beats in a given time period as well as a slower decay rate so more than three beats may be obtained even at high pressure. (c, d) Generally, large proteins will have fewer and less frequent beats as compared to smaller proteins. Moreover, when analyzing higher-charge states of a large protein (c), these highly charged ions will decay at a greater rate compared to lower-charged ions of the same molecular weight (d). Collectively, these characteristics make the need for low pressure in the UHV critical to obtaining three beats for such large molecular weight species.

Extending the mass range of Orbitrap CCS measurements

To extend Orbitrap CCS measurements to larger proteins, first we examined three proteins from 19 kDa to 29 kDa under denaturing conditions, resulting in highly charged monomeric ions of low *m/z*. These ions fall in the same *m/z* region as our prior study[38] that explored proteins ranging from 7 to 17 kDa in charge states from 5+ to 22+ and which exhibited CCS values from 1,271 to 4,920 $Å^2$. The CCS values for the three new proteins in a large variety of charge states are shown in **Figure S3a-c**. Some of the proteins in the present study, namely D1T10 (10+ to 21+) and carbonic anhydrase (15+ to 33+), displayed significantly larger CCSs (5,432 to 8,142 $Å^2$) than those measured in our previous studies.[38,44]

The differences in CCS values measured by ion mobility and Orbitrap transient decay are plotted as percent differences (ΔCCS%) in **Figure 1**. As seen by the trends in **Figure S3a-c** and **Figure 1**, the CCSs of the denatured proteins (high charge states, *m/z* values below 2,200) generally show good agreement with ion mobility CCSs (ΔCCS% values ranging from 15-1%, **Tables S2-S8**, and averaging 5% ± 3%). The

CCS values of these protein ions span a large range, 3,500 to 8,000 $Å^2$. These ions exhibited at least three beats distinguishable from the baseline despite their fast signal decay rates, even at low trapping gas pressure. When we attempted to extend the mass range up to 66 kDa (BSA, bovine serum albumin), we found that while these ions had similar *m/z* values to those just described (*m/z* 2,000 to 3,000 for charge states 23+ to 33+), the more massive and highly charged BSA ions had a much longer beat period. This meant that the signal decayed to the baseline prior to observation of three beats (**Figure S2)**, preventing the determination of CCS values. Given these results, we estimate the Orbitrap CCS limit for denatured protein ions to be about 40 kDa. However, this limit could change for different Orbitrap systems based on the lower pressure limit and collision gas used.

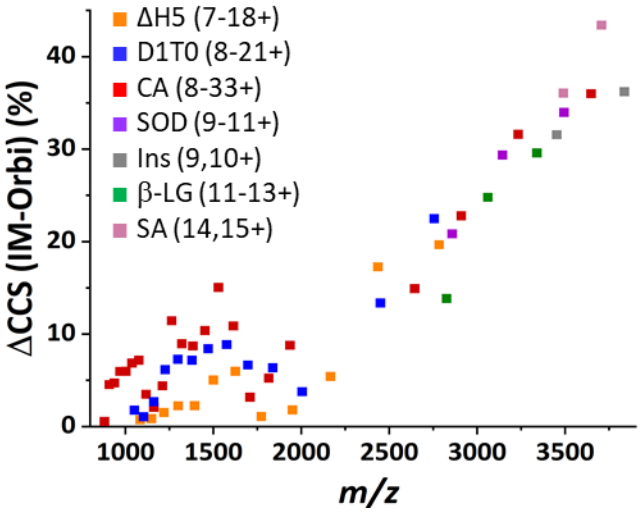

Figure 1. Difference in CCS values (ΔCCS%) obtained by Orbitrap and ion mobility measurements for seven proteins: ΔH5 (19 kDa monomer), D1T0 (22 kDa monomer), carbonic anhydrase (CA, 29 kDa monomer), superoxide dismutase (SOD, 32 kDa dimer), insulin (Ins, 34 kDa hexamer), beta lactoglobulin (β-LG, 36 kDa dimer), and streptavidin (SA, 52 kDa tetramer).

After successful measurements of CCS values for the larger denatured proteins in high charge states (*m/z* < 2,200), we focused on extending the method to lower charge states of the same proteins sprayed from aqueous solutions of high ionic strength to preserve native-like structures (*i.e.*, compact, folded, *m/z* > 2,200). In addition, several multimeric protein complexes were added to the data set. Upon examining these proteins in lower charge states, the CCS values measured by the Orbitrap method diverged notably form ones determined by IM (**Figure S3, Tables S2-S8**). The Orbitrap CCSs were routinely lower than the IM CCS values, and the discrepancy increased as the charge state decreased. The trend between the difference in CCS values measured by the two methods (*i.e.*, ΔCCS%) and charge states is notably apparent in **Figure 1**, particularly evident as the *m/z* value exceeds 2,200. A second trend emerges

when evaluating the divergence in CCS values as a function of protein mass; the disparity is greater for more massive proteins at higher *m/z* values as more massive proteins have higher ΔCCS% values than less massive proteins in the same charge state. To probe the factors that contribute to these trends, we launched an investigation into the ion dynamics of the Orbitrap as detailed below.

Kinetic Energy and Center-of-Mass Collision Energy

As noted in the introduction, CCS values measured at high kinetic energy in an Orbitrap mass analyzer are not expected to exactly match the CCS values determined by ion mobility owing to the different collision regime models. However, what is particularly interesting is the increasing divergence in the correlation as the *m/z* increases. The increasing divergence may be related to the core assumption of the Orbitrap CCS method. The primary assumption is that a single collision between an ion and a neutral gas molecule (*i.e.*, N_2) in the Orbitrap analyzer results in the removal of the ion from the ion packet owing to either scattering or fragmentation. Because the difference in CCS between IM and Orbitrap methods increases with protein mass and decreases with charge state, it suggests that some of the larger proteins are surviving some collisions, thus impeding their removal from the ion packet and yielding CCS values lower than expected. Based on the results shown in **Figure 1** and **Tables S2-8**, ion charge influences the CCS measurements too. The kinetic energy imparted to an ion before injection to the Orbitrap analyzer from the C-trap is the product of the potential difference (U_0) between the C-trap and the Orbitrap outer electrode and the ion's charge (z).[37] When an ion is oscillating inside the analyzer, the ion's kinetic energy changes with time depending on the oscillation phase. It reaches the maximum when an ion approaches the central electrode and the minimum in the vicinity of the outer electrode as illustrated in **Figure S4**. The kinetic energy (*K*) is, generally, a quasi-periodic function of time (t) determined by the potential distribution $\varphi(Z, R)$ and the axial and radial oscillations in the Orbitrap analyzer (equation 5).

$$K(t) = ez \times \{U_0 - \varphi(Z(t), R(t))\} \quad (5)$$

The kinetic energy remains proportional to the charge state (z). When the ion collides with a molecule of buffer gas with mass m_g (whose thermal velocity is substantially below the ion's velocity), the energy in the center-of-mass reference frame (E_{cm}) is inversely proportional to the *m/z* ratio, which accounts for the lower probability of dissociation for ions with higher *m/z* as described by equation 6.

$$\mathrm{E_{cm}} = \frac{m_g}{m+m_g} K \cong e\{U_0 - \varphi(Z, R)\} \times \frac{z m_g}{m} \quad (6)$$

The collision events are random, as are also the coordinates Z and R of the point where the collision occurs. If a collision happens close to the outer electrode where the kinetic energy is minimal,

the ion has a greater chance of surviving the collision without dissociation, while a collision close to the central electrode is more likely to cause dissociation or scattering, thus removing the ion from the packet. This mixed ion dissociation and survival leads to some signal decay, but not as much as expected, thus producing underestimation in CCS.

As shown in the theoretical ion path in **Figure S4**, the ion's kinetic energy oscillates in the range 3-6 keV per unit charge, and the mean center-of-mass collision energy (E_{mean},averaged for all positions around the Orbitrap) is about $4.5\ keV$ per unit charge. For lower *m/z* ions around *m/z* ~1,000 in the 10+ charge state (a typical charge state of a native protein), the mean center-of-mass collision energy is therefore approximately $\frac{Zm_g}{m} \times E_{mean} \approx\ 125\ eV$ (for experiments using nitrogen buffer gas). Based upon previous collision induced dissociation (CID) studies, protein ions subjected to $\geq$ 100 eV center-of-mass collision energies are likely to dissociate.[54] For higher *m/z* ions around *m/z* ~4000 in the 10+ charge state, the estimated $E_{mean} \approx 30\ eV$ is substantially lower, and as previously described, ions at these lower center-of-mass collision energies (< 50 eV) begin to deviate from the assumption of inevitable dissociation upon a collision.[37]

The change in the kinetic energy throughout the ion's path in the Orbitrap analyzer means that an ion may, in theory, survive the lower energy collisions encountered near the terminal ends of the Orbitrap analyzer but may decay if the collision occurs near the center of the Orbitrap analyzer. The fact that the dissociation probability is lower at least for a fraction of the ion path (**Figure S4**) will suppress signal decay and yield a lower-than-expected decay constant and hence lower apparent CCS. To evaluate the trend in CCS relative to an ion's kinetic energy and mass, the center-of-mass collision energy and minimum kinetic energy were plotted as a function of the difference between the IM CCS and Orbitrap CCS values in **Figures 2** and **S5**. The center-of-mass collision energy accounts for an ion's kinetic energy relative to the mass of the ion and neutral (equation 5), and this parameter is useful to estimate whether an ion will survive a collision in experiments involving different proteins and collision gases. The ion's minimum kinetic energy was selected rather than the mean or maximum kinetic energy because the minimum kinetic energy is most likely to lead to collisions that do not remove the ion from the ion packet and cause the deviations in the measured decay constants and CCS values.

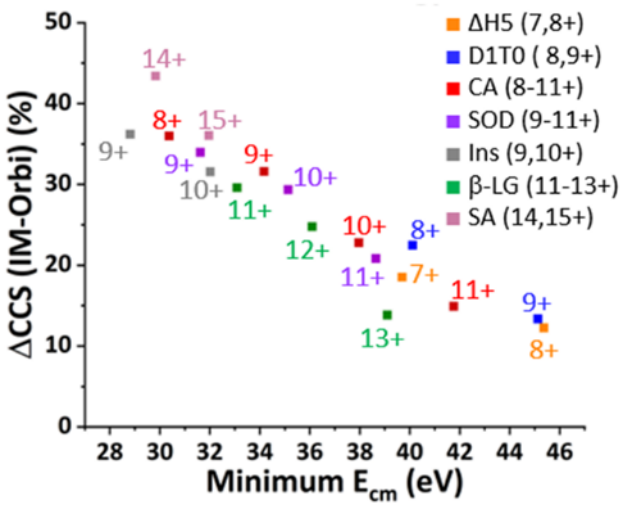

Figure 2. Difference in CCS values obtained by ion mobility versus Orbitrap measurements for proteins in low charge states as a function of the center-of-mass collision energy (E_{cm}). The data points for each of seven proteins in two to four charge states are indicated by colored-coded squares, including ΔH5 (19 kDa monomer), D1T0 (22 kDa monomer), carbonic anhydrase (CA, 29 kDa monomer), superoxide dismutase (SOD, 32 kDa dimer), insulin (Ins, 34 kDa hexamer), beta lactoglobulin (β-LG, 36 kDa dimer), and streptavidin (SA, 52 kDa tetramer).

As expected, the lower charge states of each protein show a dependence between minimum kinetic energy and ΔCCS% (**Figure S5**) owing to the increased chance of ion survival at lower kinetic energies. We found that this relationship was generally linear. Another trend emerges when considering ΔCCS% relative to the mass of the protein: for different proteins in the same charge state—the more massive protein displays the greater ΔCCS%. The kinetic energy of an ion in an Orbitrap analyzer is only dependent on its charge (approximately 4 keV per charge), so the ion's mass also must affect the ΔCCS% of the low charge states. To investigate the role of protein mass in ΔCCS%, the minimum kinetic energies were also used to calculate the corresponding center-of-mass collision energies shown in **Figure 2**, a parameter that considers both mass and charge (equation 5). When viewing ΔCCS% as a function of the center-of-mass collision energy, a near-linear trend is evident among all proteins in low charge states. ΔCCS% decreases as minimum E_{cm} increases (**Figure 2**). Above a threshold E_{cm} value (about 50 eV for the proteins considered here), ΔCCS% is always 15% or lower and typically less than 7% at higher values of E_{cm}, thus agreeing with ΔCCS% found for smaller protein ions in our previous studies (**Figure S6**).[38,44] For proteins in these higher charge states, each collision results in ion decay, leading to low ΔCCS%.

As seen in **Figure S5**, linear correlations between charge states of each protein show a negative slope and therefore the amount of kinetic energy needed to attain ΔCCS% equal to zero can be

determined by finding the x-intercept for each protein in **Figure S5**. This kinetic energy threshold can be used to ensure that each collision results in ion loss, *i.e.* if the hard or modified hard sphere collision model should be followed. To find the threshold kinetic energy for each protein, we performed linear regression for each protein in **Figure S5**. The x-intercept of this linear regression was used to estimate the threshold kinetic energy to obtain ΔCCS% equal to zero as a function of protein mass (**Figure S7**). The same work-up is shown as threshold center-of-mass collision energy relative to protein mass in **Figure 3**. All points in **Figure 3** cluster around a center-of-mass collision energy of approximately 50 eV. Collisions with energies below 50 eV are not expected to follow the hard sphere model, where every ion neutral collision results in loss of ion signal, and instead CCSs of ions in this collision energy regime should be determined using the modified hard sphere collision model as described below.

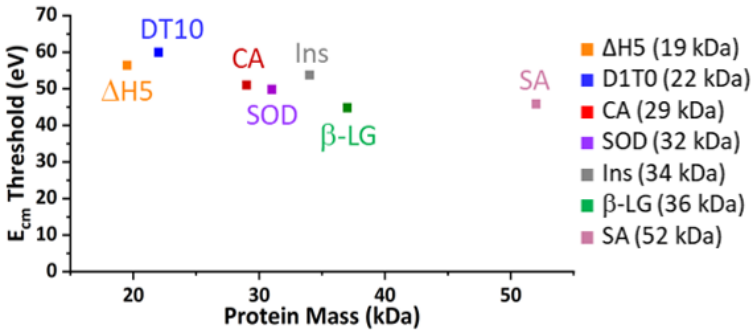

Figure 3. The center-of-mass collision energy (E_{CM}) threshold for transition to modified hard sphere collision model relative to the protein mass for seven proteins, ΔH5 (19 kDa monomer), D1T0 (22 kDa monomer), carbonic anhydrase (CA, 29 kDa monomer), superoxide dismutase (SOD, 32 kDa dimer), insulin (Ins, 34 kDa hexamer), beta lactoglobulin (β-LG, 36 kDa dimer), and streptavidin (SA, 52 kDa tetramer). Each point represents an x-intercept value from linear regression of each protein trend in in **Figure 2**. The values in these graphs correspond to conditions for which a single collision results in removal an ion from the ion packet.

Examination of **Figures 1** and **S3** indicates that the ΔCCS values increase significantly above *m/z* 2,200, with the Orbitrap CCS values consistently lower than those determined by IM, indicating that the hard sphere collision model is not followed for ions with these high *m/z* values. In essence, Orbitrap CCS values for ions below *m/z* 2,200 mirror IM CCS values within ~10% or less, and CCSs for ions above *m/z* 2,200 are underestimated. This trend enables a clear, practical delineation of the *m/z* regions where Orbitrap CCSs are (or are not) accurate as shown by the dashed lines separating the two regions in **Figure S3a-c**. To measure CCS values of ions above *m/z* 2,200 that more closely match IM CCS values, experimental and/or hardware modifications are required, such as using a heavier collision gas (to

increase the center-of-mass collision energy) or increasing the accelerating voltage employed to transfer ions from the C-trap to the Orbitrap analyzer. These two modifications would better ensure that ions will not survive any collisions and thus will exhibit predicable decay rates that correlate with CCS. We also note that while ions that survive collisions do not dissociate, changes in their tertiary structure and therefore CCS may still occur, but these possible conformational changes cannot be measured using our ensemble ion method that produces a single CCS for the entire population of ions.

The CCS values for the ions that do not follow the hard sphere collision model (*i.e*. those above *m/z* 2,200) can be corrected after acquisition of the transients. To account for the large ΔCCS seen for those ions in the modified hard sphere collision regime, a linear fit was applied to all data points in **Figure 2**, and this fit was used to correct the CCSs of lower charge states as described in more detail in Supporting Information. With this correction factor, the ΔCCS% values are reduced to 7.5% or less for all lower charge states of the six proteins, and the trend between CCS values measured by the two methods shows good agreement in **Figure 4**.

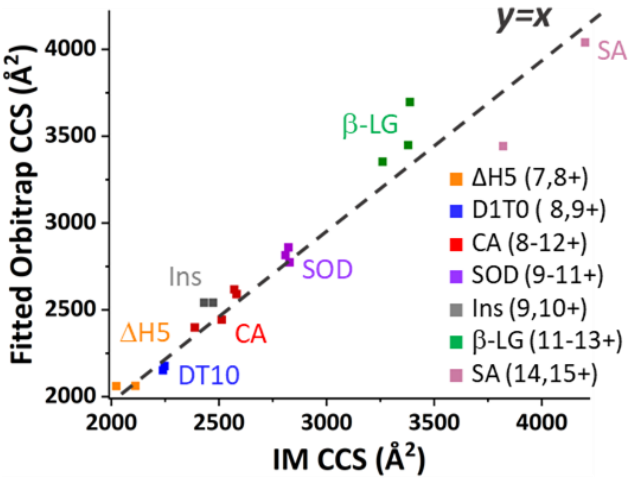

Figure 4. Fitted Orbitrap CCSs versus IM CCSs for low charge states of all six proteins. Orbitrap CCSs were fit based on linear regression in **Figure 2** to account for the difference between hard sphere vs modified hard sphere collision models. The fitting method and correction factor are described in Supporting Information.

Applications of Orbitrap CCS measurements for native proteins

After development of the fitted Orbitrap CCS method, we extended the method to probe structural changes of proteins in various native MS experiments. One example entails measuring variations in the conformations of proteins subjected to collisional induced unfolding (CIU),[11] in which collisional activation is used to thermally heat the protein prior to estimation of CCS values. CIU is typically

undertaken on an ion mobility platform, but the increasing popularity of Orbitrap systems for native MS studies[55–57] suggests that CIU would be a useful auxiliary method. We applied Orbitrap CCS measurements to monitor structural changes in carbonic anhydrase (9+) while performing in-source collisional activation, allowing isolation of the precursor ion after CIU and prior to transient decay analysis. Orbitrap CCSs were corrected to account for the deviation in hard sphere collision model (*i.e.* this ion was in the modified hard sphere regime) as described in the supplemental information. The resulting CIU curve is shown in **Figure 5**, and the CCS increases by 25% during the unfolding process prior to reaching a plateau around 2858 Å^2. The CIU curve is similar to ones measured by ion mobility, in which the increase in CCS during CIU frequently ranges from 30-50%.[58–62]

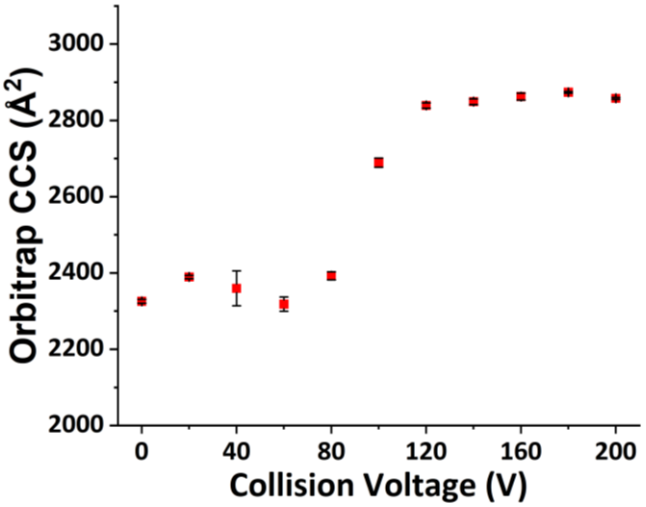

Figure 5. Orbitrap CCS of native-like carbonic anhydrase (9+, 29 kDa monomer, *m/z* 3233) relative to the collision energy used for in-source collisional activation to cause collisional heating. CCS was corrected for modified hard sphere regime collisions using the correction factor method described in the supplementary information. The error bars represent the standard deviations from three replicate measurements.

We also investigated CCSs of sub-units ejected from protein complexes. Various tandem mass spectrometry methods, including CID, ultraviolet photodissociation (UVPD), and surface induced dissociation (SID) have been used to monitor the disassembly of multimeric protein complexes as a means to infer the architecture and characterize the constituents of the macromolecular assemblies.[63–65] In addition to producing sequence ions from backbone cleavages of the proteins, these activation methods often eject monomers or other subunits (*e.g.*, dimers, trimers) from the complexes. The monomers in particular may be released as highly charged, elongated structures (a particularly prevalent process for CID) or may retain more compact native-like structures (more common for SID or UVPD) depending on

the activation method used. We first measured the CCS of monomers ejected from insulin, a hexameric assembly (MS1 spectrum in **Figure S8a**), which primarily releases individual monomers (3+) upon UVPD or HCD of the hexamer (10+). The resulting CCS values were similar for the monomers (3+) released upon UVPD or HCD (823 $\pm$ 2 Å^2 or 820 $\pm$ 3 Å^2, respectively, **Figure S8b,c**) and for the monomer observed in the MS1 spectrum of the native solution (837 $\pm$ 5 Å^2) (**Figure S8d**). This agreement is expected as insulin has 3 disulfide bonds that provide structural stability and prevent extensive unfolding of each monomer. All CCSs for the insulin monomer in the present study also agree well (within ~10%) with a previously reported IM value of 743 Å^2 (3+ monomer).[66] The CCS of the hexameric insulin assembly (10+ charge state) was 2542 $\pm$ 14 Å^2, and thus the CCS of one individual monomer is approximately 32% of the size of the hexamer.

CCS values were also measured to evaluate the disassembly of tetrameric streptavidin, a complex without any disulfide bonds. The native MS^1 spectrum is dominated by the 14+ charge state (**Figure 6a**), and the resulting CCS found with the correction factor as described for ions in the modified hard sphere collision regime in the supplementary information is 3443 $\pm$ 117 Å^2 (**Table S8**), in comparison to the previously reported CCS value of 3420 $\pm$ 40 Å^2 measured by ion mobility.[67] CID and UVPD of the 14+ tetramer primarily causes release of monomers in the 5+ and 6+ charge states (**Figure 6b,c**). The resulting CCS values of the monomer (5+ charge state) measured by the Orbitrap transient decay method are 1468 $\pm$ 6 Å^2 (HCD) and 1478 $\pm$ 3 Å^2 (UVPD), both showing reasonable agreement with the CCS calculated for the crystal structure of the monomer (1527 Å^2)[68] as well as the CCS of the monomer ejected by collisional activation and measured by IM (1325 Å^2, *Escherichia coli*).[68] The 6+ monomer released upon UVPD or HCD showed a significantly more extended conformation than the 5+ monomer, yielding CCS values of 1921 $\pm$ 11 Å^2 (UVPD) or 1934 $\pm$ 19 Å^2 (HCD). These results are consistent with a prior study that reported a CCS of 1710 Å^2 for the 6+ monomer ejected by collisional activation and measured by IM.[68] Because the species of streptavidin was different for the present study (*Streptomyces avidinii*) versus the prior study (*Escherichia coli*),[68] the CCS values are not expected to be identical. In-source collisional dissociation was also used to disassemble the streptavidin tetramers, and the CCS values of the released monomers were 1426 $\pm$ 9 Å^2 for the 5+ monomer (**Figure 6d**) and 1840 $\pm$ 7 Å^2 for the 6+ monomer (**Figure 6e**), both values slightly lower (3-4%) than the CCSs obtained for the corresponding monomers released upon HCD or UVPD.

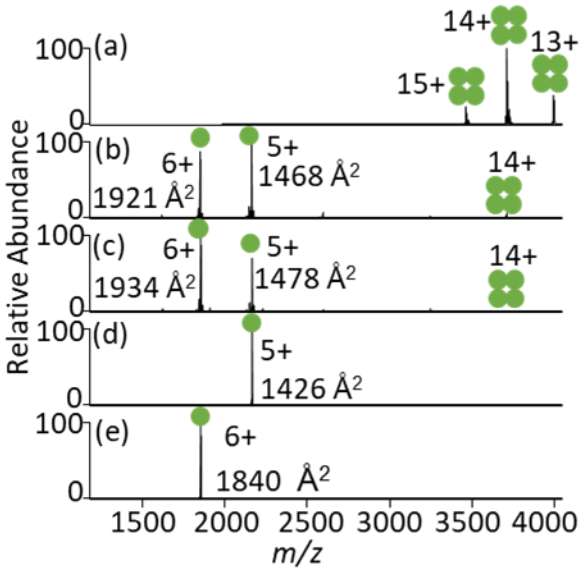

Figure 6. Mass spectra obtained for tetrameric streptavidin and resulting CCS values. a) MS^1 spectrum, b) UVPD (1 pulse, 1 mJ) of 14+ charge state, c) HCD (50 CE) of 14+ charge state, and in-source CID (80 eV) and isolation of d) 5+ monomer or e) 6+ monomer.

Conclusion:

When extending Orbitrap CCS measurements to larger proteins, we first showed that these measurements are reasonably accurate for denatured protein ions below *m/z* 2,200. However, when analyzing the same proteins in lower charge states, we found that Orbitrap measurements systematically underestimated the CCS values. The energy of collision of the ion and neutral in the Orbitrap analyzer was found to be the cause of underestimation, with insufficient collision energy allowing ion survival instead of decay. The underestimation in CCS increases as the center-of-mass collision energy decreases. Guidelines were established for the *m/z* regions where CCSs are accurate, and a correction factor was established for the *m/z* regions in which the CCS values diverge. We demonstrated the utility of this method by monitoring protein unfolding, and we measured the CCS of monomers ejected from protein complexes using collisional dissociation and ultraviolet photodissociation. The methods explored in this study may be considered as a strategy to evaluate the retention of folded protein structures under different solution conditions or after activation. Additionally, the discovery of the collision energy at which ion survival occurs is key in understanding ion dynamics within the Orbitrap analyzer, information that may help develop more robust future generations of Orbitraps and inform those exploring new frontiers of the Orbitrap including single ion studies. Adoption of a modified hard collision model opens intriguing

possibilities of probing secondary and tertiary structures of molecules which are not accessible to traditional IMS.

Supporting Information

A description of the correction factor used for underestimated CCSs, additional graphs showing the relationships between ion energy, position in the Orbitrap, Orbitrap CCS deviation, and ion *m/z*, as well as tables of CCS values obtained by IM and Orbitrap CCS measurements are provided.

Declaration of competing interest

The authors declare the following financial interests which may be considered as potential competing interests: four authors (Aizikov, Fort, Grinfeld, Makarov), are employees of Thermo Fisher Scientific, the manufacturer of the Orbitrap mass spectrometer used for the study.

Acknowledgments

We acknowledge the following funding sources: NSF (Grant CHE-2203602) and the Welch Foundation (Grant F-1155). Deseree Reid and Michael Marty are gratefully acknowledged for providing ΔH5 and D1T0 protein. The template plasmid, pMSP1D1 (D1T0), was a gift from Stephen Sligar (Addgene plasmid no. 20061), and ΔH5 was a gift from Gerhard Wagner (Addgene #71714).

References

(1) Dodds, J. N.; Baker, E. S. Ion Mobility Spectrometry: Fundamental Concepts, Instrumentation, Applications, and the Road Ahead. *J. Am. Soc. Mass Spectrom.* **2019**, *30* (11), 2185–2195. https://doi.org/10.1021/jasms.8b06240.

(2) Poltash, M. L.; McCabe, J. W.; Shirzadeh, M.; Laganowsky, A.; Russell, D. H. Native IM-Orbitrap MS: Resolving What Was Hidden. *TrAC Trends Anal. Chem.* **2020**, *124*, 115533. https://doi.org/10.1016/j.trac.2019.05.035.

(3) Zhong, Y.; Hyung, S.-J.; Ruotolo, B. T. Ion Mobility–Mass Spectrometry for Structural Proteomics. *Expert Rev. Proteomics* **2012**, *9* (1), 47–58. https://doi.org/10.1586/epr.11.75.

(4) Ruotolo, B. T.; Benesch, J. L. P.; Sandercock, A. M.; Hyung, S.-J.; Robinson, C. V. Ion Mobility–Mass Spectrometry Analysis of Large Protein Complexes. *Nat. Protoc.* **2008**, *3* (7), 1139–1152. https://doi.org/10.1038/nprot.2008.78.

(5) Harris, R. A.; Leaptrot, K. L.; May, J. C.; McLean, J. A. New Frontiers in Lipidomics Analyses Using Structurally Selective Ion Mobility-Mass Spectrometry. *TrAC Trends Anal. Chem.* **2019**, *116*, 316–323. https://doi.org/10.1016/j.trac.2019.03.031.

(6) Stow, S. M.; Causon, T. J.; Zheng, X.; Kurulugama, R. T.; Mairinger, T.; May, J. C.; Rennie, E. E.; Baker, E. S.; Smith, R. D.; McLean, J. A.; Hann, S.; Fjeldsted, J. C. An Interlaboratory Evaluation of Drift Tube Ion Mobility–Mass Spectrometry Collision Cross Section Measurements. *Anal. Chem.* **2017**, *89* (17), 9048–9055. https://doi.org/10.1021/acs.analchem.7b01729.

(7) Kanu, A. B.; Dwivedi, P.; Tam, M.; Matz, L.; Hill, H. H. Ion Mobility–Mass Spectrometry. *J. Mass Spectrom.* **2008**, *43* (1), 1–22. https://doi.org/10.1002/jms.1383.
(8) May, J. C.; Jurneczko, E.; Stow, S. M.; Kratochvil, I.; Kalkhof, S.; McLean, J. A. Conformational Landscapes of Ubiquitin, Cytochrome c, and Myoglobin: Uniform Field Ion Mobility Measurements in Helium and Nitrogen Drift Gas. *Int. J. Mass Spectrom.* **2018**, *427*, 79–90. https://doi.org/10.1016/j.ijms.2017.09.014.
(9) Smith, D. P.; Knapman, T. W.; Campuzano, I.; Malham, R. W.; Berryman, J. T.; Radford, S. E.; Ashcroft, A. E. Deciphering Drift Time Measurements from Travelling Wave Ion Mobility Spectrometry-Mass Spectrometry Studies. *Eur. J. Mass Spectrom.* **2009**, *15* (2), 113–130. https://doi.org/10.1255/ejms.947.
(10) Salbo, R.; Bush, M. F.; Naver, H.; Campuzano, I.; Robinson, C. V.; Pettersson, I.; Jørgensen, T. J. D.; Haselmann, K. F. Traveling-Wave Ion Mobility Mass Spectrometry of Protein Complexes: Accurate Calibrated Collision Cross-Sections of Human Insulin Oligomers: Traveling-Wave IM-MS of Protein Complexes. *Rapid Commun. Mass Spectrom.* **2012**, *26* (10), 1181–1193. https://doi.org/10.1002/rcm.6211.
(11) Dixit, S. M.; Polasky, D. A.; Ruotolo, B. T. Collision Induced Unfolding of Isolated Proteins in the Gas Phase: Past, Present, and Future. *Curr. Opin. Chem. Biol.* **2018**, *42*, 93–100. https://doi.org/10.1016/j.cbpa.2017.11.010.
(12) Hernandez, D. R.; DeBord, J. D.; Ridgeway, M. E.; Kaplan, D. A.; Park, M. A.; Fernandez-Lima, F. Ion Dynamics in a Trapped Ion Mobility Spectrometer. *Analyst* **2014**, *139* (8), 1913–1921. https://doi.org/10.1039/C3AN02174B.
(13) Michelmann, K.; Silveira, J. A.; Ridgeway, M. E.; Park, M. A. Fundamentals of Trapped Ion Mobility Spectrometry. *J. Am. Soc. Mass Spectrom.* **2015**, *26* (1), 14–24. https://doi.org/10.1021/jasms.8b04886.
(14) Chai, M.; Young, M. N.; Liu, F. C.; Bleiholder, C. A Transferable, Sample-Independent Calibration Procedure for Trapped Ion Mobility Spectrometry (TIMS). *Anal. Chem.* **2018**, *90* (15), 9040–9047. https://doi.org/10.1021/acs.analchem.8b01326.
(15) Naylor, C. N.; Reinecke, T.; Ridgeway, M. E.; Park, M. A.; Clowers, B. H. Validation of Calibration Parameters for Trapped Ion Mobility Spectrometry. *J. Am. Soc. Mass Spectrom.* **2019**, *30* (10), 2152–2162. https://doi.org/10.1007/s13361-019-02289-1.
(16) Reinecke, T.; Naylor, C. N.; Clowers, B. H. Ion Multiplexing: Maximizing Throughput and Signal to Noise Ratio for Ion Mobility Spectrometry. *TrAC Trends Anal. Chem.* **2019**, *116*, 340–345. https://doi.org/10.1016/j.trac.2019.03.014.
(17) McCabe, J. W.; Mallis, C. S.; Kocurek, K. I.; Poltash, M. L.; Shirzadeh, M.; Hebert, M. J.; Fan, L.; Walker, T. E.; Zheng, X.; Jiang, T.; Dong, S.; Lin, C.-W.; Laganowsky, A.; Russell, D. H. First-Principles Collision Cross Section Measurements of Large Proteins and Protein Complexes. *Anal. Chem.* **2020**, *92* (16), 11155–11163. https://doi.org/10.1021/acs.analchem.0c01285.
(18) Keelor, J. D.; Zambrzycki, S.; Li, A.; Clowers, B. H.; Fernández, F. M. Atmospheric Pressure Drift Tube Ion Mobility–Orbitrap Mass Spectrometry: Initial Performance Characterization. *Anal. Chem.* **2017**, *89* (21), 11301–11309. https://doi.org/10.1021/acs.analchem.7b01866.
(19) Ibrahim, Y. M.; Garimella, S. V. B.; Prost, S. A.; Wojcik, R.; Norheim, R. V.; Baker, E. S.; Rusyn, I.; Smith, R. D. Development of an Ion Mobility Spectrometry-Orbitrap Mass Spectrometer Platform. *Anal. Chem.* **2016**, *88* (24), 12152–12160. https://doi.org/10.1021/acs.analchem.6b03027.
(20) Panczyk, E.; Snyder, D.; Liu, F.; Lin, Y.-F.; Ridgeway, M.; Park, M.; Bleiholder, C.; Wysocki, V. Evaluation of a Bruker TimsTOF Pro for Native Mass Spectrometry. *ChemRxiv* **2021**. https://doi.org/10.33774/chemrxiv-2021-qr78t.

(21) Uetrecht, C.; J. Rose, R.; Duijn, E. van; Lorenzen, K.; R. Heck, A. J. Ion Mobility Mass Spectrometry of Proteins and Protein Assemblies. *Chem. Soc. Rev.* **2010**, *39* (5), 1633–1655. https://doi.org/10.1039/B914002F.
(22) Uetrecht, C.; Versluis, C.; Watts, N. R.; Wingfield, P. T.; Steven, A. C.; Heck, A. J. R. Stability and Shape of Hepatitis B Virus Capsids In Vacuo. *Angew. Chem. Int. Ed.* **2008**, *47* (33), 6247–6251. https://doi.org/10.1002/anie.200802410.
(23) Duijn, E. van; Barendregt, A.; Synowsky, S.; Versluis, C.; Heck, A. J. R. Chaperonin Complexes Monitored by Ion Mobility Mass Spectrometry. *J. Am. Chem. Soc.* **2009**, *131* (4), 1452–1459. https://doi.org/10.1021/ja8055134.
(24) Jeanne Dit Fouque, K.; Garabedian, A.; Leng, F.; Tse-Dinh, Y.-C.; Ridgeway, M. E.; Park, M. A.; Fernandez-Lima, F. Trapped Ion Mobility Spectrometry of Native Macromolecular Assemblies. *Anal. Chem.* **2021**, *93* (5), 2933–2941. https://doi.org/10.1021/acs.analchem.0c04556.
(25) Guo, D.; Xin, Y.; Li, D.; Xu, W. Collision Cross Section Measurements for Biomolecules within a High-Resolution FT-ICR Cell: Theory. *Phys Chem Chem Phys* **2015**, *17* (14), 9060–9067. https://doi.org/10.1039/C4CP06065B.
(26) Li, D.; Tang, Y.; Xu, W. Ion Collision Cross Section Measurements in Fourier Transform-Based Mass Analyzers. *The Analyst* **2016**, *141* (12), 3554–3561. https://doi.org/10.1039/C5AN02164B.
(27) Yang, F.; Voelkel, J. E.; Dearden, D. V. Collision Cross Sectional Areas from Analysis of Fourier Transform Ion Cyclotron Resonance Line Width: A New Method for Characterizing Molecular Structure. *Anal. Chem.* **2012**, *84* (11), 4851–4857. https://doi.org/10.1021/ac300379a.
(28) Jones, C. A.; Dearden, D. V. Linewidth Pressure Measurement: A New Technique for High Vacuum Characterization. *J. Am. Soc. Mass Spectrom.* **2015**, *26* (2), 323–329. https://doi.org/10.1021/jasms.8b04964.
(29) Jiang, T.; Chen, Y.; Mao, L.; Marshall, A. G.; Xu, W. Extracting Biomolecule Collision Cross Sections from the High-Resolution FT-ICR Mass Spectral Linewidths. *Phys Chem Chem Phys* **2016**, *18* (2), 713–717. https://doi.org/10.1039/C5CP02987B.
(30) Anupriya; Gustafson, E.; Mortensen, D. N.; Dearden, D. V. Quantitative Collision Cross-Sections from FTICR Linewidth Measurements: Improvements in Theory and Experiment. *J. Am. Soc. Mass Spectrom.* **2018**, *29* (2), 251–259. https://doi.org/10.1007/s13361-017-1738-4.
(31) Tang, Y.; Li, D.; Cao, D.; Xu, W. Extracting Biomolecule Collision Cross Sections from FT-ICR Mass Spectral Line Shape. *Talanta* **2019**, *205*, 120093. https://doi.org/10.1016/j.talanta.2019.06.093.
(32) Mao, L.; Chen, Y.; Xin, Y.; Chen, Y.; Zheng, L.; Kaiser, N. K.; Marshall, A. G.; Xu, W. Collision Cross Section Measurements for Biomolecules within a High-Resolution Fourier Transform Ion Cyclotron Resonance Cell. *Anal. Chem.* **2015**, *87* (8), 4072–4075. https://doi.org/10.1021/acs.analchem.5b00102.
(33) Anupriya; Jones, C. A.; Dearden, D. V. Collision Cross Sections for 20 Protonated Amino Acids: Fourier Transform Ion Cyclotron Resonance and Ion Mobility Results. *J. Am. Soc. Mass Spectrom.* **2016**, *27* (8), 1366–1375. https://doi.org/10.1007/s13361-016-1409-x.
(34) Pope, B. L.; Joaquin, D.; Hickey, J. T.; Mismash, N.; Heravi, T.; Shrestha, J.; Arslanian, A. J.; Anupriya; Mortensen, D. N.; Dearden, D. V. Multi-CRAFTI: Relative Collision Cross Sections from Fourier Transform Ion Cyclotron Resonance Mass Spectrometric Line Width Measurements. *J. Am. Soc. Mass Spectrom.* **2022**, *33* (1), 131–140. https://doi.org/10.1021/jasms.1c00297.
(35) Elliott, A. G.; Harper, C. C.; Lin, H.-W.; Susa, A. C.; Xia, Z.; Williams, E. R. Simultaneous Measurements of Mass and Collisional Cross-Section of Single Ions with Charge Detection Mass Spectrometry. *Anal. Chem.* **2017**, *89* (14), 7701–7708. https://doi.org/10.1021/acs.analchem.7b01675.

(36) Dziekonski, E. T.; Johnson, J. T.; Lee, K. W.; McLuckey, S. A. Determination of Collision Cross Sections Using a Fourier Transform Electrostatic Linear Ion Trap Mass Spectrometer. *J. Am. Soc. Mass Spectrom.* **2018**, *29* (2), 242–250. https://doi.org/10.1007/s13361-017-1720-1.
(37) Makarov, A.; Denisov, E. Dynamics of Ions of Intact Proteins in the Orbitrap Mass Analyzer. *J. Am. Soc. Mass Spectrom.* **2009**, *20* (8), 1486–1495. https://doi.org/10.1016/j.jasms.2009.03.024.
(38) Sanders, J. D.; Grinfeld, D.; Aizikov, K.; Makarov, A.; Holden, D. D.; Brodbelt, J. S. Determination of Collision Cross-Sections of Protein Ions in an Orbitrap Mass Analyzer. *Anal. Chem.* **2018**, *90* (9), 5896–5902. https://doi.org/10.1021/acs.analchem.8b00724.
(39) Giles, K.; Grimsrud, E. P. The Kinetic Ion Mobility Mass Spectrometer: Measurements of Ion-Molecule Reaction Rate Constants at Atmospheric Pressure. *J. Phys. Chem.* **1992**, *96* (16), 6680–6687. https://doi.org/10.1021/j100195a030.
(40) Langejuergen, J.; Allers, M.; Oermann, J.; Kirk, A.; Zimmermann, S. High Kinetic Energy Ion Mobility Spectrometer: Quantitative Analysis of Gas Mixtures with Ion Mobility Spectrometry. *Anal. Chem.* **2014**, *86* (14), 7023–7032. https://doi.org/10.1021/ac5011662.
(41) Covey, T.; Douglas, D. J. Collision Cross Sections for Protein Ions. *J. Am. Soc. Mass Spectrom.* **1993**, *4* (8), 616–623. https://doi.org/10.1016/1044-0305(93)85025-S.
(42) Chen, Y.-L.; Collings, B. A.; Douglas, D. J. Collision Cross Sections of Myoglobin and Cytochrome c Ions with Ne, Ar, and Kr. *J. Am. Soc. Mass Spectrom.* **1997**, *8* (7), 681–687. https://doi.org/10.1016/S1044-0305(97)00033-0.
(43) Plass, W. R.; Cooks, R. G. A Model for Energy Transfer in Inelastic Molecular Collisions Applicable at Steady State or Non-Steady State and for an Arbitrary Distribution of Collision Energies. *J. Am. Soc. Mass Spectrom.* **2003**, *14* (12), 1348–1359. https://doi.org/10.1016/j.jasms.2003.08.012.
(44) James, V. K.; Sanders, J. D.; Aizikov, K.; Fort, K. L.; Grinfeld, D.; Makarov, A.; Brodbelt, J. S. Advancing Orbitrap Measurements of Collision Cross Sections to Multiple Species for Broad Applications. *Anal. Chem.* **2022**, *94* (45), 15613–15620. https://doi.org/10.1021/acs.analchem.2c02146.
(45) Yang, F.; Jones, C. A.; Dearden, D. V. Effects of Kinetic Energy and Collision Gas on Measurement of Cross Sections by Fourier Transform Ion Cyclotron Resonance Mass Spectrometry. *Int. J. Mass Spectrom.* **2015**, *378*, 143–150. https://doi.org/10.1016/j.ijms.2014.07.026.
(46) Wörner, T. P.; Aizikov, K.; Snijder, J.; Fort, K. L.; Makarov, A. A.; Heck, A. J. R. Frequency Chasing of Individual Megadalton Ions in an Orbitrap Analyser Improves Precision of Analysis in Single-Molecule Mass Spectrometry. *Nat. Chem.* **2022**, *14* (5), 515–522. https://doi.org/10.1038/s41557-022-00897-1.
(47) Reid, D. J.; Keener, J. E.; Wheeler, A. P.; Zambrano, D. E.; Diesing, J. M.; Reinhardt-Szyba, M.; Makarov, A.; Marty, M. T. Engineering Nanodisc Scaffold Proteins for Native Mass Spectrometry. *Anal. Chem.* **2017**, *89* (21), 11189–11192. https://doi.org/10.1021/acs.analchem.7b03569.
(48) Blevins, M. S.; Juetten, K. J.; James, V. K.; Butalewicz, J. P.; Escobar, E. E.; Lanzillotti, M. B.; Sanders, J. D.; Fort, K. L.; Brodbelt, J. S. Nanohydrophobic Interaction Chromatography Coupled to Ultraviolet Photodissociation Mass Spectrometry for the Analysis of Intact Proteins in Low Charge States. *J. Proteome Res.* **2022**, *21* (10), 2493–2503. https://doi.org/10.1021/acs.jproteome.2c00450.
(49) Sanders, J. D.; Shields, S. W.; Escobar, E. E.; Lanzillotti, M. B.; Butalewicz, J. P.; James, V. K.; Blevins, M. S.; Sipe, S. N.; Brodbelt, J. S. Enhanced Ion Mobility Separation and Characterization of Isomeric Phosphatidylcholines Using Absorption Mode Fourier Transform Multiplexing and Ultraviolet Photodissociation Mass Spectrometry. *Anal. Chem.* **2022**, *94* (10), 4252–4259. https://doi.org/10.1021/acs.analchem.1c04711.
(50) Fort, K. L.; Dyachenko, A.; Potel, C. M.; Corradini, E.; Marino, F.; Barendregt, A.; Makarov, A. A.; Scheltema, R. A.; Heck, A. J. R. Implementation of Ultraviolet Photodissociation on a Benchtop Q

Exactive Mass Spectrometer and Its Application to Phosphoproteomics. *Anal. Chem.* **2016**, *88* (4), 2303–2310. https://doi.org/10.1021/acs.analchem.5b04162.
(51) Reinecke, T.; Clowers, B. H. Implementation of a Flexible, Open-Source Platform for Ion Mobility Spectrometry. *HardwareX* **2018**, *4*, e00030. https://doi.org/10.1016/j.ohx.2018.e00030.
(52) Sipe, S. N.; Sanders, J. D.; Reinecke, T.; Clowers, B. H.; Brodbelt, J. S. Separation and Collision Cross Section Measurements of Protein Complexes Afforded by a Modular Drift Tube Coupled to an Orbitrap Mass Spectrometer. *Anal. Chem.* **2022**, *94* (26), 9434–9441. https://doi.org/10.1021/acs.analchem.2c01653.
(53) Siems, W. F.; Viehland, L. A.; Hill, H. H. Improved Momentum-Transfer Theory for Ion Mobility. 1. Derivation of the Fundamental Equation. *Anal. Chem.* **2012**, *84* (22), 9782–9791. https://doi.org/10.1021/ac301779s.
(54) Mitchell Wells, J.; McLuckey, S. A. Collision-Induced Dissociation (CID) of Peptides and Proteins. In *Methods in Enzymology*; Biological Mass Spectrometry; Academic Press, 2005; Vol. 402, pp 148–185. https://doi.org/10.1016/S0076-6879(05)02005-7.
(55) Webb, I. K. Recent Technological Developments for Native Mass Spectrometry. *Biochim. Biophys. Acta BBA - Proteins Proteomics* **2022**, *1870* (1), 140732. https://doi.org/10.1016/j.bbapap.2021.140732.
(56) Boeri Erba, E.; Signor, L.; Petosa, C. Exploring the Structure and Dynamics of Macromolecular Complexes by Native Mass Spectrometry. *J. Proteomics* **2020**, *222*, 103799. https://doi.org/10.1016/j.jprot.2020.103799.
(57) Tamara, S.; den Boer, M. A.; Heck, A. J. R. High-Resolution Native Mass Spectrometry. *Chem. Rev.* **2022**, *122* (8), 7269–7326. https://doi.org/10.1021/acs.chemrev.1c00212.
(58) Borotto, N. B.; Osho, K. E.; Richards, T. K.; Graham, K. A. Collision-Induced Unfolding of Native-like Protein Ions Within a Trapped Ion Mobility Spectrometry Device. *J. Am. Soc. Mass Spectrom.* **2022**, *33* (1), 83–89. https://doi.org/10.1021/jasms.1c00273.
(59) Gadkari, V. V.; Ramírez, C. R.; Vallejo, D. D.; Kurulugama, R. T.; Fjeldsted, J. C.; Ruotolo, B. T. Enhanced Collision Induced Unfolding and Electron Capture Dissociation of Native-like Protein Ions. *Anal. Chem.* **2020**, *92* (23), 15489–15496. https://doi.org/10.1021/acs.analchem.0c03372.
(60) Phetsanthad, A.; Li, G.; Jeon, C. K.; Ruotolo, B. T.; Li, L. Comparing Selected-Ion Collision Induced Unfolding with All Ion Unfolding Methods for Comprehensive Protein Conformational Characterization. *J. Am. Soc. Mass Spectrom.* **2022**, *33* (6), 944–951. https://doi.org/10.1021/jasms.2c00004.
(61) Zheng, X.; Kurulugama, R. T.; Laganowsky, A.; Russell, D. H. Collision-Induced Unfolding Studies of Proteins and Protein Complexes Using Drift Tube Ion Mobility-Mass Spectrometer. *Anal. Chem.* **2020**, *92* (10), 7218–7225. https://doi.org/10.1021/acs.analchem.0c00772.
(62) Sipe, S. N.; Lancaster, E. B.; Butalewicz, J. P.; Whitman, C. P.; Brodbelt, J. S. Symmetry of 4-Oxalocrotonate Tautomerase Trimers Influences Unfolding and Fragmentation in the Gas Phase. *J. Am. Chem. Soc.* **2022**, *144* (27), 12299–12309. https://doi.org/10.1021/jacs.2c03564.
(63) N. Sipe, S.; S. Brodbelt, J. Impact of Charge State on 193 Nm Ultraviolet Photodissociation of Protein Complexes. *Phys. Chem. Chem. Phys.* **2019**, *21* (18), 9265–9276. https://doi.org/10.1039/C9CP01144G.
(64) Greisch, J.-F.; Tamara, S.; A. Scheltema, R.; R. Maxwell, H. W.; D. Fagerlund, R.; C. Fineran, P.; Tetter, S.; Hilvert, D.; R. Heck, A. J. Expanding the Mass Range for UVPD-Based Native Top-down Mass Spectrometry. *Chem. Sci.* **2019**, *10* (30), 7163–7171. https://doi.org/10.1039/C9SC01857C.
(65) Harvey, S. R.; Ben-Nissan, G.; Sharon, M.; Wysocki, V. H. Surface-Induced Dissociation for Protein ComplexProtein Complexes Characterization. In *Proteoform Identification: Methods and Protocols*; Sun, L., Liu, X., Eds.; Methods in Molecular Biology; Springer US: New York, NY, 2022; pp 211–237. https://doi.org/10.1007/978-1-0716-2325-1_15.

(66) Raja, U. K. B.; Injeti, S.; Culver, T.; McCabe, J. W.; Angel, L. A. Probing the Stability of Insulin Oligomers Using Electrospray Ionization Ion Mobility Mass Spectrometry. *Eur. J. Mass Spectrom.* **2015**, *21* (6), 759–774. https://doi.org/10.1255/ejms.1396.
(67) Laszlo, K. J.; Bush, M. F. Interpreting the Collision Cross Sections of Native-like Protein Ions: Insights from Cation-to-Anion Proton-Transfer Reactions. *Anal. Chem.* **2017**, *89* (14), 7607–7614. https://doi.org/10.1021/acs.analchem.7b01474.
(68) S. Quintyn, R.; R. Harvey, S.; H. Wysocki, V. Illustration of SID-IM-SID (Surface-Induced Dissociation-Ion Mobility-SID) Mass Spectrometry: Homo and Hetero Model Protein Complexes. *Analyst* **2015**, *140* (20), 7012–7019. https://doi.org/10.1039/C5AN01095K.

For table of contents only